

PAPER REF: 7131

A FINITE ELEMENT MODEL TO STUDY WELD AND GEOMETRIC IMPERFECTIONS IN AN IMPACT ATTENUATOR DEVICE

J.A. López-Campos^(*), A. Segade¹, E. Casarejos¹, J.R. Fernandez², J.A. Vilán¹

¹Department of Mechanical Engineering, University of Vigo, E-36310 Vigo, Spain

²Department of Applied Mathematics I, University of Vigo, E-36310 Vigo, Spain

^(*)*Email:* joseangellopezcampos@uvigo.es

ABSTRACT

Energy absorbers of safety systems in vehicles are typically mechanical parts. These parts are designed to crush adequately under impact, removing part of the kinetic energy as strain. The mechanical parts are usually formed including welded joints, however the study of these parts does not include the welding failure as a design concern. During an impact test of an attenuator we could observe the failure of one welded edge. We defined a finite element (FE) model to describe the impact test. We used the technique of trigger deformation to obtain a model that replied the folding pattern observed. The acceleration time profile was also reasonably described. The FE model produced the gap opening at the edge in the right location, as observed, probing that the strain provided by the model at the welded joints are realistic. We made a systematic study of the influence of the trigger location, as well as point defects at the welding joint and rigidity weakening in wider regions. We found that the acceleration profile was only influenced by the plying pattern. The causes we input to force a possible welding failure did not cause any important change, but for the case it affected the starting of the plying process.

Keywords: impact attenuator, crashworthiness, welding, non-linear FEM, LS-DYNA, buckling initiator

1. INTRODUCTION

Passive safety in vehicles is based mostly in the modifying the behaviour of the structure under impact. For that purpose there are parts designed to have a better control on the local rigidity. These parts are useful by absorbing the impact (kinetic) energy while deforming under loads to produce strain energy, and reduce the energy reaching other vehicle parts. The location of these parts on the vehicle imposes different requirements. The cross-beam in the bumpers requires bending and lateral deformations; the front-rail, axial and oblique deformations; and for the side panels, bending deformations. Despite their very different purposes and aspects, these elements are named under their function as impact absorbers.

Impact attenuators (IA) are typically designed by using thin-walled structures (Baroutajia, 2017). This preferred design is based on the good dynamical behaviour, production feasibility and cost-effectiveness of various applied solutions. The axial crushing of these structures causes failure either by global (Euler), progressive, or (dynamic) plastic buckling. For dynamic plastic buckling it is necessary to generate a uniform stress over the entire axial length of the part, so that radial displacements are uniformly produced over the whole axial length and there are not bending moments caused by these displacements. However, in

progressive buckling the formation of plies do not happen over all the length of the component, and buckling is located at specific zones. The preferred option is designing to achieve progressive buckling because more energy is absorbed due to larger amount of material deformed plastically.

Thin-walled IAs were studied considering constant section geometries squared (Abramowicz, 1984) and circular (Abramowicz, 1986), and tapered sections rectangular (Reid, 1986) and conical (Zhang, 2014). Fusta show a better behaviour under oblique impacts. A detailed study of tapered structures and the influence of cross-section, wall thickness, angles, etc. was made by (Guler, 2010).

The actual buckling and folding of one structure under an applied load, even if the location and direction of the load is well determined, depends on the geometrical deviations, material in-homogeneities and residual stresses. These different causes are rather unpredictable and may be quoted as ‘imperfections’, which strongly define the buckling of thin-walled structures (Langseth, 1999). Otherwise, the structures may include defaults made in purpose to cause a designed failure (Yuen, 2008; Hirose, 2014).

Despite the obvious necessity of including welding in the production of most of these structures, most of the studies do not consider the possible influence of welding on the buckling behaviour. Welding will cause stresses that can influence the buckling (Somodi, 2017). The quality of the welding, if including defects, will act as buckling trigger location. In this work we wanted to address the possible influence of the welding in the performance of the IAs. We studied the case of an absorber designed for application under the rules of Formula-SAE vehicles (SAE, 2017). It is an IA located at the front part and designed for axial impact. Some characteristics and the influence of the materials were described in (Segade, 2016). For this study we considered the original material (aluminium alloy) with high specific energy absorption, and made with welded parts.

This work is organized as follows. First we describe axial-crush test applied to the IA. Then we describe the FE model developed to describe the test and the type of trigger we used to reproduce the folding. In the next part we describe the influence of the trigger location on the load profile, and select one case to obtain a realistic model. Finally we analysed the influence caused by forcing different defaults, both local and extended, related to the welding edges.

2. IMPACT TEST

The test used as reference in this work was done with an impact absorber designed for implementation into a SAE-Formula car. The geometry is a truncated tapered pyramid of rectangular section. The size accomplishes with the rules of SAE-Formula to be within a given envelope ($L \times W \times H$, 270.3 x 159.8 x 234.5 mm³) with restrictions on the angles, and then adapted to the specific vehicle. The thin wall part was made of aluminium alloy (EN AW 5083-O) sheet (2.5 mm thickness) and formed by welding the four sides and the front lid. An additional flange at the opposite side was used for connection, but has no interest in this study.

The IA was tested in a drop tower (at CTAG-IDIADA Safety Technology, Spain) to check the energy absorption characteristics of the part (Segade, 2016). As specified by the same rules the minimum energy was established in 7350 J. The test was performed by dropping an impact block of 348 kg released at 2.13 m above the IA to achieve 6.47 m/s at the impact point. The test was recorded by a high-speed camera (1000 FPS) and one accelerometer

(Kyowa Electronic Instruments) set at the impact block. The acceleration data were analysed by a Channel Filter Class CFC-60 (100 Hz) according to norm SAE-J211. The IA was hit in axial (vertical) direction, fixed at the bottom flange to the test bench. The high-speed pictures showed the folding pattern of the structure while crushing. It was possible also to observe a failure in one edge causing a gap (Figure 3). At the end of the crushing the part height was about 60 mm, 25.6% of the initial size (height of 234.5 mm). The maximum acceleration peaks were measured at 8 ms (14.85g) and 46 ms (28.8 g). The average acceleration value was 9.96g in a time spam of about 60 ms. The acceleration time profile details will be discussed later in relation with the analysed data.

3. FINITE ELEMENT MODEL OF THE IA AND TEST

We built a Finite Element model to reproduce the load behaviour shown by the real impact attenuator device. In the model we reproduced the test details as close as possible (geometry and loads). To solve the analysis we used the commercial code LS-DYNA (R8.1.0, Livermore Software Technology Corp. CA, USA), adequate to deal with the dynamic problem including the strong non-linearity, by using an explicit approach to the problem.

The model contains three parts (bodies), two for the impact block and the bench support, and one for the IA. The impact block and bench were defined as rigid surfaces, with a coarse mesh. The bench part was fixed. The block included mass elements to define the inertial mass of the test, and defined with the initial speed at impact time. Gravity effects were also included to add the extra effect on the (vertical) test.

The IA was modelled with the actual geometry and meshed (mapped mesh) with shell elements of size 5 mm (Figure 1). The elements (2.5 m thickness) had 5 integration points across the thickness in order to accurately compute the bending moments, especially when the section reaches the yield range. The element size was selected with a mesh sensitive analysis, by performing several calculations to evaluate the proper description of the crushed plies and the convergence of the results.

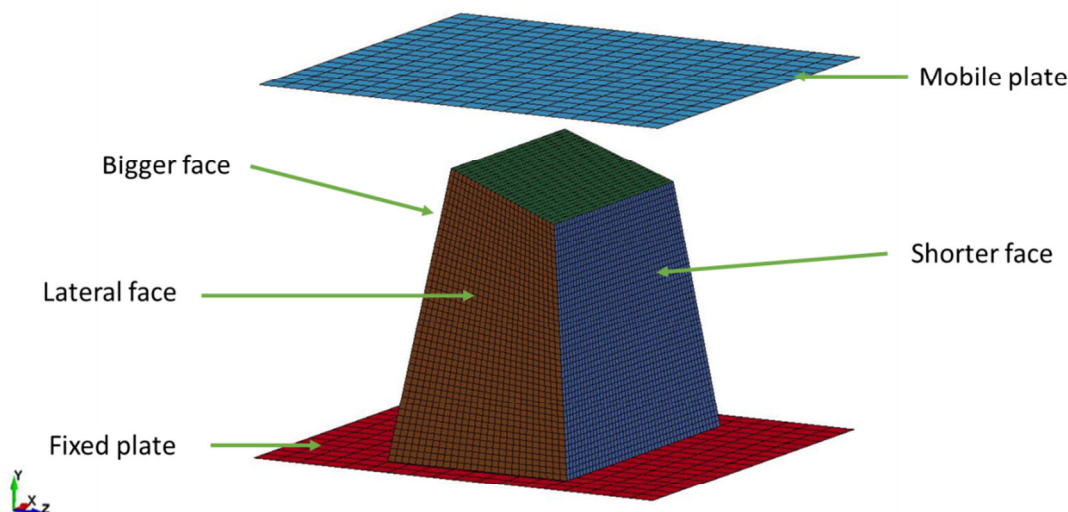


Fig. 1 - Drawings of the parts included in the FE model including the meshes: coarse mesh for the rigid surfaces, one fixed and one mobile; and 5 mm sized elements for the IA. The IA is within an envelope (LxWxH) of 270.3 x 159.8 x 234.5 mm³.

For our studies we wanted a model capable to reproduce the reference test. This situation is different of designing a part to reproduce an optimized load pattern under impact, which can be achieved with pre-deformed shapes introduced to the original structure (Segade, 2018: these proceedings). For our purpose we used the method of introducing a default in the mesh pattern, therefore forcing the plying sequence to start preferably at the selected location, or at least to influence the folding pattern. By inspection of the plying sequence observed in the pictures of the test, we introduced the default in the bigger surfaces, located at different heights in the horizontal plane. The default was an inward deviation of the mesh nodes in the same horizontal line, being null at the edges and following a cosine shape with a single maximum at the middle position (Langseth, 1999). The deviation was set to reproduce adequately the first initial peak (Langseth, 1999; Zarei, 2006).

The aluminium alloy EN AW 5083-O used for IA was defined as a material with elasto-plastic properties included in an isotropic hardening plasticity model. The material parameters are listed in Table 1 according (Segade, 2016).

Table 1 - Mechanical properties of the aluminium alloy (EN AW 5083-O) used in the FE model

| | |
|----------------------------|-------------------------|
| Elastic Modulus | 72 GPa |
| Yield Strength | 115 MPa |
| Tangent Modulus | 1.082 |
| Density | 2 700 kg/m ³ |
| Poisson Coefficient | 0.33 |

The IA body was composed of five different plates welded at the edges in a corner joint by fillet welding. To characterize this joining we used a specific LS-DYNA parameterisation dedicated to include in the simulation the welded joints of the parts. This feature defines the welding stress state and possible failure according to the fillet geometry and the strength of the material involved. For the fillet the width, length and plate thickness are required. In our case the width was 3 mm, defined by the filler metal rod used for fabrication (2.4 mm). The length depends on the distance between nodes located at the edges, and may vary depending on each edge (5.3 - 4.5 mm) due to the mapped mesh. The thickness was that of the plates (2.5 mm). The definition of the welding is done node-to-node, a method that provides with large flexibility in the model definition but it is largely time consuming. We used a MATLAB (The MathWorks, MA, USA) routine to directly re-write the LS-DYNA cards to input the modifications we needed into the nodes corresponding to the welded edges. The strength of the weld fillet was defined as 260 MPa according to (Mutombo, 2010).

The contact between the folded plies, including self-contact, was defined using a penalty formulation. After the simulations were completed, we check either for penetrations or missed contacts to re-adjust the penalty conditions. The crushing process lasts for about 60 milliseconds, from impact until the mass is fully stopped. During the computation, the acceleration of the impacting mass was recorded in 0.5 ms steps. The acceleration time profile will be used to compare the behaviour of the different models studied and also with respect to the data obtained in the test. Each model computation requires about 28 minutes in a processor Intel-Core i7-4820K 64Gb RAM. The model will be first studied to produce the observed folding pattern by introducing a trigger in the geometry.

4. TRIGGER LOCATION

We analysed the influence of the location of the trigger by evaluating models defined with different initial locations, and comparing with the test results. The evaluated locations were set at different horizontal positions, considering as ‘vertical’ the natural direction in the test bench and corresponding to the axial direction of the impact, Y-axis in Figure 1. The locations were at the upper, middle and lower third regions in both the bigger and the shorter faces (not in the lateral ones). The plies, however, were analysed by inspecting the lateral faces, to compare with the images obtained during the crushing test (Figure 1). Several test were used to evaluate the (maximum) deviation needed by the trigger definition according to the results, and it was set to the working value of 1 mm. This value does not refer to any actual deformation geometry, but reflects only the effects of the true imperfections that would cause the folding observed.

In Figure 2 we plot the acceleration time profile measured (line A) as well as the values obtained varying the trigger location from the upper third (line B), to the middle third (line C) and lower third (line D) in the face with higher height. In the test data we can see a broad peak (15g) till 20 ms, a constant plateau (7.5g) between 20 and 32 ms and the higher peak (26g) between 32 and 60 ms. This profile corresponds to a first peak generated in the initial unstable situation prior to the folding of the structure. Then, while plying, the load decreases and stabilises. Once the structure is crushed and the plies are touching each other the load increases again due to the extra rigidity till the energy is exhausted.

About the calculations, the results corresponding to the trigger at the upper location are the more realistic (line B). The time spam is similar (55 ms) to the measured data; the first peak is reproduced in value and position, and there is a plateau before the final load increase. However there are more oscillations, the initial peak is narrower, and the second one is broader and reaches a lower value (23g). The same characteristics are observed in any calculated case, so they are model-dependent. For the cases with the trigger at the other positions (lines C and D), the first peak increases and delays, the plateau disappears and the second peak happens too early, reducing the time spam considerably. The fact that the trigger be located farther in the axial crushing process helps little to smooth the loads in the initial time range.

We also evaluated the results by locating the trigger in the shorter face of the IA, again at three different heights. The results were rather similar to the previous cases with the trigger located in other position than the upper third, and the values (almost) coincide with those of the line C in Figure 2. Definitely, only if the trigger is located in the upper part of the longer face do affects to the plying pattern, and thus to the acceleration profile. Otherwise, the trigger is useless because the folding is already developed, and the stiffness changes due to the plying pattern in the crushing process are defined before the trigger can induce any appreciable modification.

In Figure 3 there is a time sequence of the crushing process comparing both the test pictures in real time and the results obtained with the trigger located in the upper part of the longer face (corresponding to line B in Figure 2). We can observe that the plying pattern is reproduced rather closely both in time and shape. Any other location of the trigger in the models caused a rather different folding pattern, rather similar in all cases, and resulting in the similar acceleration curves discussed above. The higher acceleration observed in the model after 25 ms (Figure 2) is due to the self-contact caused by the plies in the shorter face. At this time-point, all plies are developed, and any differences between plies in the model and part accumulate the contact effects to make a difference in rigidity in the final stage of the crushing.

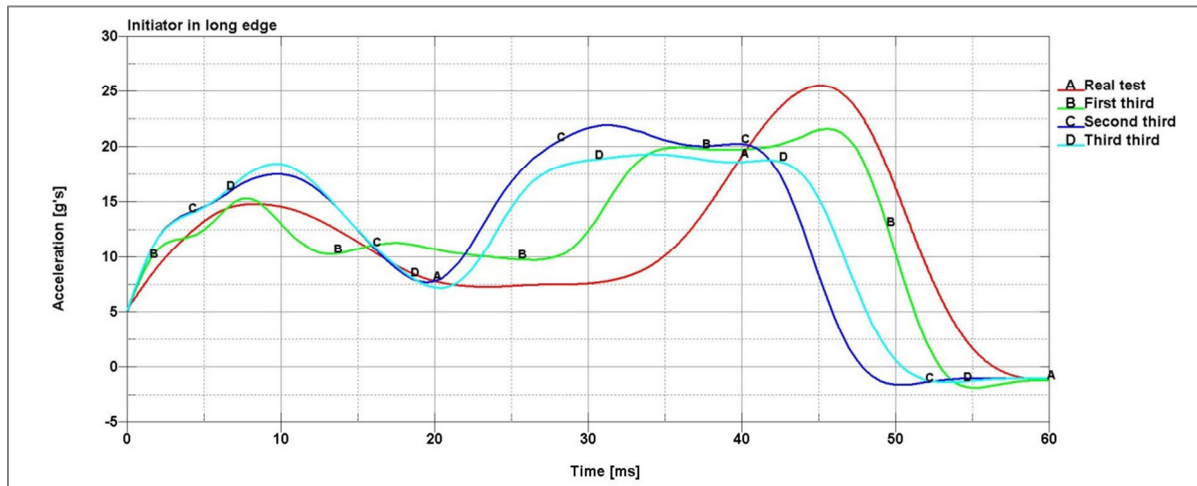


Fig. 2 - Acceleration profile measured during the axial crushing test (line A). The evaluated results are plot for the cases with the trigger located in the longer face at the upper third (line B), middle third (line C) and lower third positions (line D).

In the third sequence in Figure 3 we can observe (marked) that a gap was formed in one of the edges. The stress was high enough at the plied corner that the welding failed and the plates were set apart. This effect can be reproduced by the calculations in a completely natural way. This gap is present in any calculation whatever the conditions of trigger, if the plying reaches a similar condition. Therefore, we conclude that the stress states at the welding lines are reliable data as developed in the model.

5. INFLUENCE OF WELD DEFAULTS

We studied two possible failure cases affecting a local or a wide region of the welded edges. First we analysed a model defined so that the joint between two nodes is lost. This has a quite limited extension (about 5 mm), and can be thought as caused by a welding defect which caused a crack-like default. By setting this node-to-node default at different heights of the edges (upper, middle and lower regions of both the higher and shorter edges), we observed that all cases produced rather similar results and the acceleration profiles were close in shape and values to line B of Figure 2. Only if the default was set close to the position of the deformation trigger, the acceleration profile slightly changed, but not appreciably modifying the results.

A different analysis was done considering that a wider region, corresponding to one third of the edge, had a lower strength (60% of the original value). This situation can be seen as a general failure of the welding joint during the production. In Figure 4 we plot the acceleration time profile considering the default located at different regions of the longer edge. We analysed also the cases by setting the wide weakening default at the shorter edges. The acceleration time profiles were rather similar. Only if the default was set at the upper third of the edge the load profile changes, just slightly if located in the shorter edge, but largely if located in the longer edge, line B in Figure 4. Now, the change is important, with a large oscillation in the 15-35 ms range, reaching an important maximum value, but never exceeding the maximum (final) peak value.

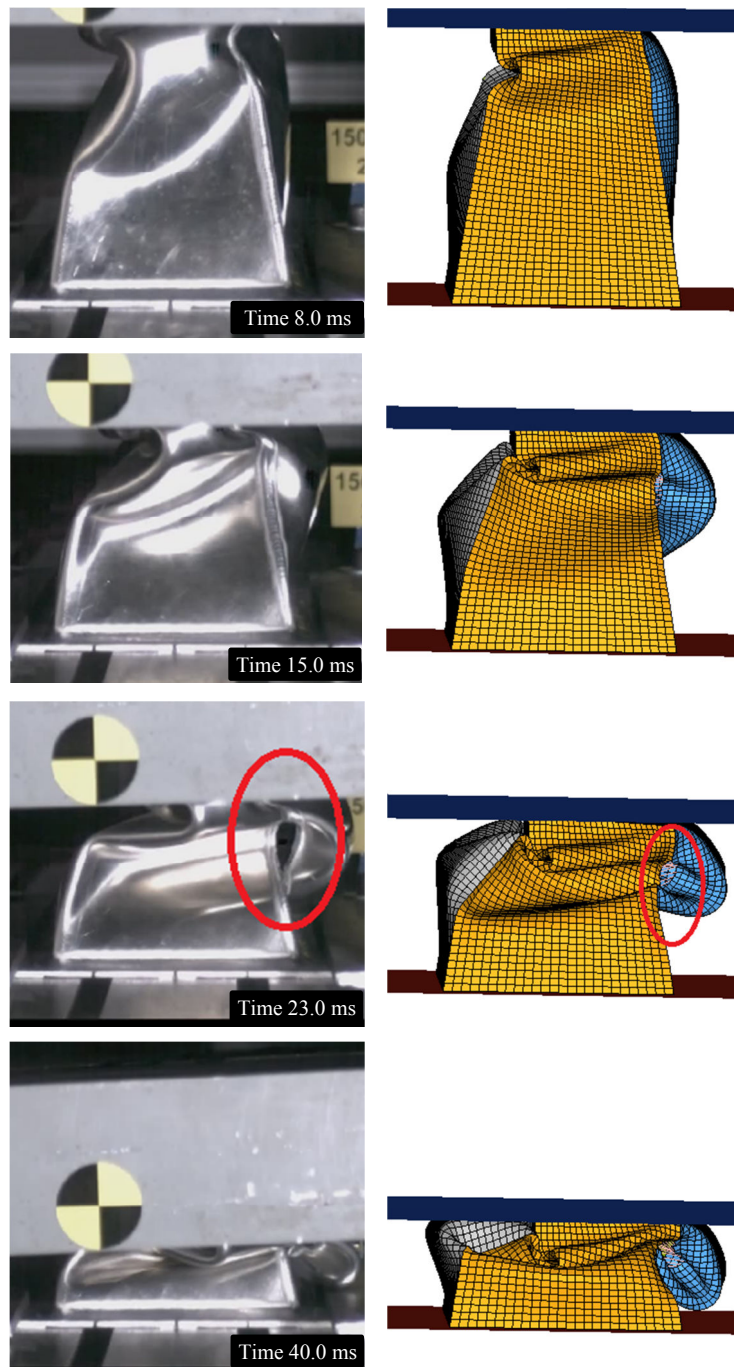


Fig. 3 - Time sequence of the crushing process.

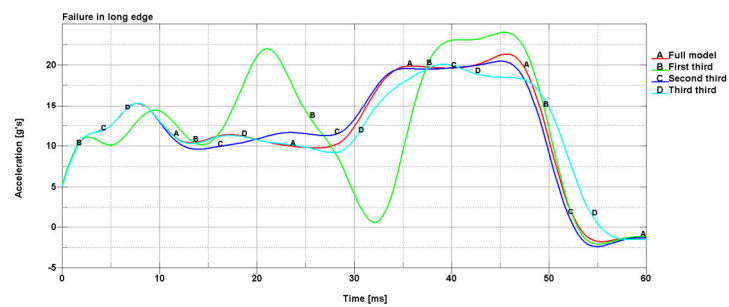


Fig. 4 -Acceleration time profiles corresponding to model evaluations.

This different pattern happens because the welding default corresponds with the location of the deformation trigger. The effect was not important in the case with the local welding default at that position, even if some small change was produced. This important difference can be easily understood by looking to the Figure 5.

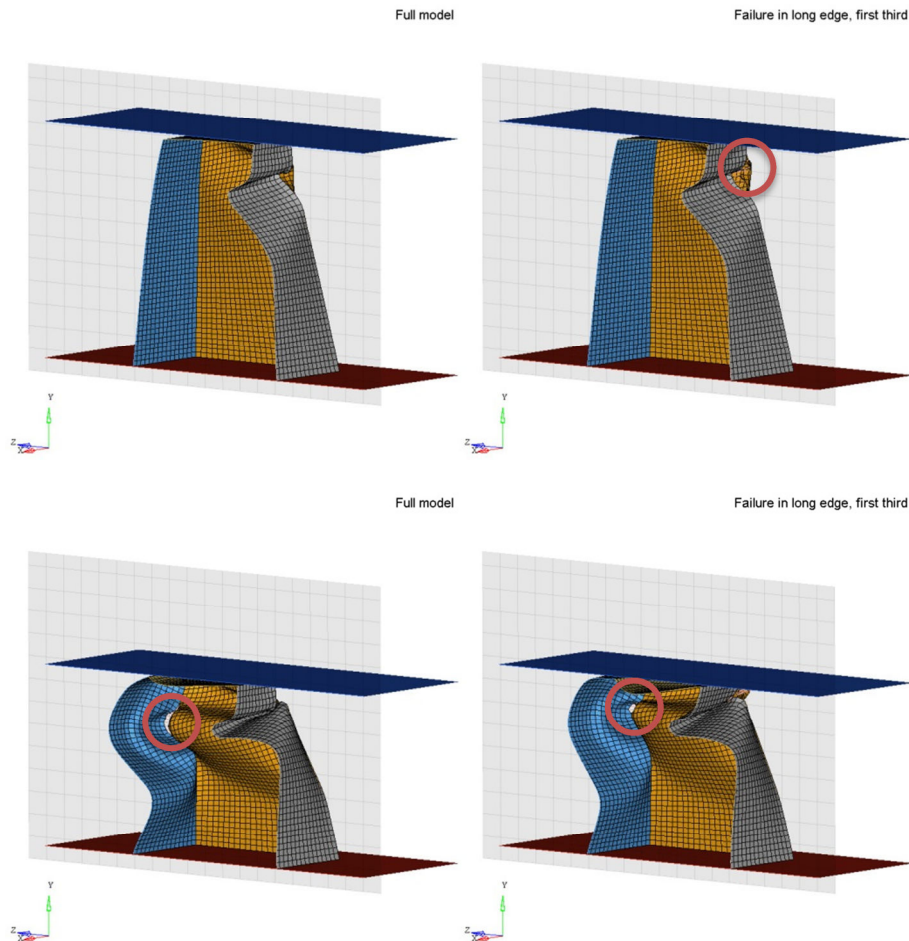


Fig. 5 - Drawings of a cross section of the IA during the crushing process.

The drawings correspond to the model with the deformation trigger located at the upper third (left column) and the extra welding default in the upper part of the edge (right panels). In the upper panels, at time 6 ms, we can observe a gap formed in the initial plies if the welding is weak, but not present in normal conditions. This failure causes the lower peak of line B (Figure 4) in the initial 5 ms. At 15 ms (lower panels), the expected gap appears additionally. The new contacts in the plies cause the differences in stiffness in the rest of the time spam.

We also investigated if this default could be equivalent (and justify) the deformation trigger. Removing the trigger and setting the welding default at the upper region of the longer edge, the result was similar to lines C and D of Figure 2. The plying pattern is ruled by the geometry and the influence of the weakened welding makes not big differences.

It is important to note that in all the cases analysed there is a failure caused by the open gap at the edge (see Figure 3). If the plying pattern is defined, the stress at the edge causes that failure, and it is not related to any weakening situation.

6. CONCLUSION

This work was motivated to analyse the influence of the welding joint quality into the design of impact attenuators of vehicle energy absorbers. We built a FE model to reproduce the impact test of an attenuator tested in a drop tower. The attenuator included a set of welded joints. The FE model reproduced satisfactory both the (measured) acceleration time profile and the welding failure observed in the test.

The model included a deformation trigger to control the plying pattern. We could verify that the acceleration profile is completely ruled by the plying pattern, and this pattern is only influenced if the trigger was located at a defined region. Otherwise, the pattern is different and has a lower correspondence with the measured case.

With this FE model we could study the influence of welding failures. We tested small local failures, which caused very limited changes. We also tested wide weakened-strength regions. In this case, only if the weakening region and deformation trigger were close, the acceleration profile changed notably. We could relate that change to the failure of the welded joint and local gap opening. However if the weakening effect was at any other region, the plying pattern is not influenced and therefore the acceleration time-history is almost unchanged.

We also investigated if the welding weakening could explain the deformation trigger. But the welding alone did not modify the plying pattern, and the result differed from the test. These results point clearly that the welding defaults have a limited influence in the crushing description of thin walled attenuators, ruled by buckling processes. Small welding defaults seem to be negligible. Only if a wide welding weakening combines with more complex 'defaults' that define the buckling process, the result is affected. We observed then more important load (acceleration) oscillations, but not increased maximum peaks nor different time spans.

In this situation we conclude that if welding inspection is considered important, it should be focused in determining weakened strength in wide regions. If the buckling pattern were forced (Segade, 2018: these proceedings), the inspection would be located at the pre-defined regions. Otherwise, if this type of defect was present, it would only have influence in some cases, and the influence would not drastically change the attenuator functionality.

ACKNOWLEDGMENTS

The work of J.R. Fernández was partially supported by the Ministerio de Economía y Competitividad (Spain) under the research project MTM2015-66640-P (with FEDER Funds).

E. Casarejos, J.A. López-Campos, A. Segade and J.A. Vilán gratefully acknowledge the funding by Xunta de Galicia (Spain) under the program Grupos de Referencia Competitiva with Ref. GRC2015/016.

J.A. López-Campos also acknowledges the funding from the Xunta de Galicia (Spain) under the program Axudas de apoio a etapa predoutoral with Ref. ED481A-2017/045.

REFERENCES

[1] Abramowicz W, Jones N. Dynamic axial crushing of square tubes. *International Journal of Impact Engineering*, 1984, 2, pp. 179-208.

- [2] Abramowicz W, Jones N. Dynamic progressive buckling of circular and square tubes. *International Journal of Impact Engineering*, 1986, 4, pp. 243-270.
- [3] Baroutajia A, Sajjiab M, Olabic AG. On the crashworthiness performance of thin-walled energy absorbers: Recent advances and future developments. *Thin-Walled Structures*, 2017, 118, pp. 137-163.
- [4] El-Hage H, Mallick PK, Zamani N. A numerical study on the quasistatic axial crush characteristics of square aluminum tubes with chamfering and other triggering mechanisms. *International Journal of Crashworthiness*, 2005, 10 (2), pp. 183-196.
- [5] Guler MA, Cerit ME, Bayram B, Berçeker B, Karakaya E. The effect of geometrical parameters on the energy absorption characteristics of thin-walled structures under axial impact loading, *International Journal of Crashworthiness*, 2010, 15 (4), pp. 377-390.
- [6] Hirose S. Shock absorbing member. Patent PCT No.: PCT/JP2012/070109 Feb.7, 2014.
- [7] Langseth M, Hopperstad OS, Berstad T. Crashworthiness of aluminium extrusions: validation of numerical simulation, effect of mass ratio and impact velocity. *International Journal of Impact Engineering*, 1999, 22, pp. 829-854.
- [8] Mutombo K, du Toit M. Mechanical properties of 5083 aluminium welds after manual and automatic pulsed gas metal arc welding using E5356 filler. *Material Science Forum*, 2010, 654-656, pp. 2560-2563.
- [9] Reid SR, Reddy TY. Static and dynamic crushing of tapered sheet metal tubes of rectangular cross-section. *International Journal of Mechanical Sciences*. 1986, 28 (9), pp. 623-637.
- [10] SAE 2017. 2017 - 2018 Formula SAE Rules. SAE International: Warrendale, PA, USA, 2017. Available online: <https://www.fsaonline.com> (accessed on 29 March 2018).
- [11] Segade A, López-Campos JA, Fernández JR, Casarejos E, Vilán JA. Finite element simulation for analysing the design and testing of an energy absorption system. *Materials* 2016, 9, pp. 660 1-13.
- [12] Segade A, Bolaño A, López-Campos JA, Casarejos E, Fernandez JR, Vilán JA. Study of a crash box design optimized for an uniform load profile. *Proceeding of the 6th International Conference Integrity-Reliability-Failure*. 2018, Lisboa.
- [13] Somodi B, Kovesdi B. Flexural buckling resistance of welded HSS box section members. *Thin-Walled Structures*, 2017, 119, pp. 266-281.
- [14] Yuen S.C.K., Nurick G.N., The energy-absorbing characteristics of tubular structures with geometric and material modifications: an overview. *Applied Mechanics Reviews Transactions of the ASME*, 2008, 61 (2), pp. 020802 1-15.
- [15] Zarei HR, Kroger M. Multiobjective crashworthiness optimization of circular aluminum tubes, *Thin-Walled Structures*, 2006, 44, pp. 301-308.
- [16] Zhang Y, Sun G, Xu X, Li G, Li Q. Multiobjective crashworthiness optimization of hollow and conical tubes for multiple load cases, *Thin-Walled Struct*, 2014, 82, pp. 331-342.